International Journal of Energetica (IJECA)
https://www.ijeca.info
ISSN: 2543-3717 Volume 6. Issue 1. 2021
Page 25-33

Effect of Rain on the Aerodynamic Performance of a Horizontal Axis Wind Turbine – A Computational Study

Eleni Douvi*, Dimitra Douvi, Dimitrios Pylarinos, Dionissios Margaris

Department of Mechanical Engineering and Aeronautics, University of Patras, GREECE

Email: douvi.eleni@gmail.com*

Abstract *–This paper analyzes numerically the impact of rainfall on the aerodynamic performance of a three-bladed Horizontal Axis Wind Turbine, with blades constructed by NACA 4418 airfoil. The simulations were conducted by the help of the commercial Computational Fluid Dynamics code, ANSYS Fluent 19.2. Firstly, the optimum geometry of the blade was designed with an application based on Blade Element Momentum theory. The Moving Reference Frame Model was applicated to simulate the rotation of the blades and the k-ω shear-stress transport turbulence model was added as well. The simulation of rain was accomplished by the Discrete Phase Model and the Taylor Analogy Breakup model was enabled to simulate droplets breakup. Three different rainfall conditions were studied, corresponding to Liquid Water Contents of 10g/m³, 30g/m³ and 60g/m³. The influence of droplet diameter on the aerodynamic performance of the blade was also examined. The results showed that the aerodynamic performance of the wind turbine is degraded in rain conditions, and the degradation is greater for higher values of Liquid Water Content and for larger diameter of water droplets.*

Keywords: *Aerodynamic Performance, Discrete Phase Model, Horizontal Axis Wind Turbine, Rainfall.*

Received: 06/06/2021 – Accepted: 26/06/2021

I. Introduction

Energy demand and consumption in modern societies is increasing recently by 2.3%, approximately twice the average rate of increase since 2010 [1]. Electricity is mainly generated by fossil fuels burning, which is responsible for greenhouse gasses emissions.

Renewable energy sources (RES) are vital against climate change. By 2050, the greenhouse gas emissions in EU should be at least 80 lower than 1990 levels. In order to achieve this goal, renewable energy technologies for power generation, such as wind turbines, have to be implemented [2]. There are many types of wind turbines, but the Horizontal Axis Wind Turbines (HAWTs) have prevailed, as they demonstrate higher power coefficients.

According to 2019 statistics from the World Wind Energy Association (WWEA), the installed capacity of wind turbines worldwide exceeded 650 GW [3]. Wind turbines operate in open environment, thus they are exposed in hazard weather conditions, i.e. extreme winds, ice accumulation and rain, which not only cause damages to the machine [4], but they affect their aerodynamic performance as well [5].

Recent developments in computing power have led to the efficiency improvement of wind energy industry, since simulations replaced the costly experiments. The majority of these studies deal with the selection of appropriate locations for wind turbine installation in complex terrain. The recent trends on numerical methods applied in wind energy industry were reviewed [6] and it was concluded that greater accuracy is accomplished when coupling different methods. A numerical model, called RIAM-COMPACT, was developed in order to estimate the real airflow over complex terrain [7]. The numerical results were validated by comparing them with flow measurements from Noma Wind Park, so it can be concluded that RIAM-COMPACT can accurately predict the airflow over complex terrain. The WAsP model and Computational Fluid Dynamics methods were utilized in order to predict the airflow over a cliff on the north of island of Madeira, where there is an interest of wind park installation, and finally select the most appropriate location for wind turbines [8]. A particle tracking model for wind turbine wake flow estimation was also proposed [9]. The advantages of the model are that it is more accurate for complex terrain than the former linear model and it can also generate optimum wind turbines layout. Moreover, the proper computational procedure in order

to simulate the flow over complex terrain, by the help of a three-dimensional Reynolds-averaged Navier–Stokes solver with k–ω turbulence model was recommended [10].

The effect of blade geometry on the performance of wind turbines was investigated computationally as well. A user-friendly software for large scale wind turbines blade optimization was developed [11]. In particular, the shape of the blades is optimized, and the aerodynamic performance is analyzed. The results showed that after optimization, the thrust coefficient reduced by 7.5% and the overall efficiency enhanced by 1%. The aeroelastic behavior of wind turbine blade sections, taking into account the airfoil radial position and the rotational speed of the blade was simulated as well [12]. The aeroelastic stability of wind turbine blades is crucial, since is more likely for cracks to be created on them. Furthermore, the optimum angle of attack for untwisted wind turbine blades, in order to maximize power output was examined computationally [13]. It was concluded that the optimum angles of attack are those angles that exhibit the highest lift coefficients. The optimum wind turbine blade geometry, i.e. chord length and twist angle, was also investigated [14]. Two different airfoils were examined, NACA 4410 and NACA 2415, and it was concluded that the power output is maximized for angles of attack with highest lift coefficient, as well. Blades are constructed from various airfoils and the wind turbine performance depends on the airfoil aerodynamic behavior. The presence of dust or rainfall results on aerodynamic degradation of the airfoils. The impact of the presence of sand particles over wind turbine airfoils, namely NACA 0012 [15] and S809 airfoil [16] was analyzed numerically. They concluded that the aerodynamic performance of the airfoils is degraded due to sand particles presence, and the degradation is higher for higher concentrations of sand particles and higher angles of attack. The aerodynamic performance of NACA 63415 airfoil under sand presence, at $Re=460\times10^3$ was also studied numerically and it was found out that the lift coefficient could be reduced up to 28% at sandy conditions [17].

The interest of the researchers, concerning the effects of rainfall on aerodynamic sector, was focused on the investigated on the aerodynamic performance of airplanes under these conditions [18, 19]. The rainfall over the NACA 0012 airfoil at rain rate of 1000mm/h, which corresponds to Liquid Water Content (LWC) of $30g/m^3$ and at $Re=1\times10^6$ and $Re=3\times10^6$ was simulated [20]. A year later, the aerodynamic performance of the same airfoil at $Re=1\times10^5$ and at LWCs of $20.548g/m^3$, $37.745g/m^3$, $41.096g/m^3$ and $75.491g/m^3$ was studied numerically and experimentally [21, 22]. It was found out that the aerodynamic performance degrades in rainfall due to the formation of water film on the surface of the airfoil and the cratering effects from the impact of raindrops. The degradation is higher as the angle of attack or the LWC increases. The degradation due to rain leads to less power generation of the wind turbines, as it was found experimentally [23]. Specifically, it was found that the performance of the NASA Mod-0 HAWT was degraded by 20% for light rain and by 30% for heavy rain.

The aerodynamic performance of a three-bladed HAWT with blades constructed by NACA 4418 airfoil under rainfall is examined in this paper. The blade geometry is the optimum, derived by the Blade Element Momentum (BEM) theory [24] and its behavior was simulated by the help of the commercial Computational Fluid Dynamics (CFD) code, ANSYS Fluent 19.2 [25]. Firstly, the operation of the blade under air flow was analyzed and then, different rainfall conditions were examined, in order to show the impact of rain droplets on the aerodynamic performance of the wind turbine. It was concluded that rain affects the aerodynamic performance of the wind turbine. In particular, the power coefficient of the wind turbine is decreased as the Liquid Water Content and the droplet diameter increase.

II. Computational Analysis

II.1. Horizontal Axis Wind Turbine Blade Geometry

Prior to the computational simulation, the blade of the three-bladed Horizontal Axis Wind Turbine had to be designed. The optimum geometry of the blade was calculated by TTBEM, an application based on the Blade Element Momentum (BEM) theory originally developed for tidal turbines, but it can be applicated for HAWTs as well [26]. The blade was constructed by NACA 4418 airfoil which is characterized by high lift to drag ratio, in order to achieve high aerodynamic performance. The length of the blade is 40m and the selected Tip Speed Ratio (TSR) is equal to 6, a typical value for three-bladed HAWTs. The data provided from TTBEM were then inserted in Qblade open source software [27], to create the three-dimensional geometry file of the blade as shown in Figure 1.

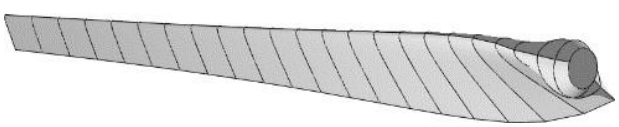

Figure 1. The blade geometry

II.2. Computational Simulation

The simulations for both one phase flow and two-phase flow cases were conducted by the commercial CFD code ANSYS Fluent 19.2.

The next step in the process is to create the computational domain around one blade, a one third of a truncated cone, placed horizontally. Periodic boundary conditions, with a periodicity of 120 degrees, are applied in order to include in the simulation procedure the remaining two blades of the rotor. The hub and the tower of the HAWT are not taking into account, since their effect on the aerodynamic behavior of the rotor is insignificant.

The front side of the truncated cone is placed 90m upstream the blade, has a diameter of 120m and is defined as velocity inlet. The lateral side is located 180 downstream the blade, its diameter is 240m and is defined as pressure outlet. The computational domain and the boundary conditions are presented in Figure 2.

A grid independence study was conducted, and it was found that the most appropriate mesh for the simulation consists of about one million (1.000.000) cells. The mesh is hybrid, and in particular, it is structured on the blade, a proper inflation was added over the blade, and unstructured in the remaining domain. Close to the blade, were greater accuracy is necessary, the mesh is denser as shown in Figure 3.

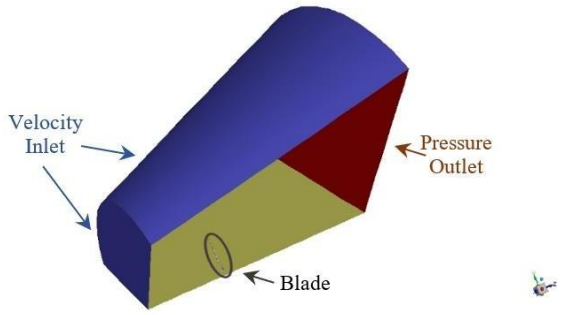

Figure 2. The computational domain and the boundary conditions

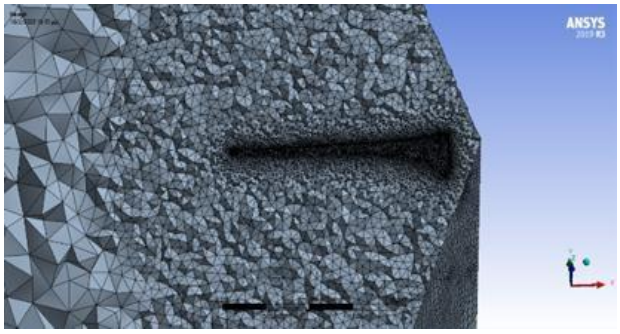

Figure 3. The computational mesh close to the wind turbine blade

All the simulations were conducted for an air velocity equal to 15m/s, which is a usual air velocity for wind turbines operation.

The rotation of the blades was simulated by the help of Moving Reference Frame Model (MRF) [28] and the most appropriate turbulence model for such simulations is the k-ω shear-stress transport (SST) [29], which can accurately predict the separation of the boundary layer under adverse pressure gradient. The ratio of average velocity fluctuations to average velocity is expressed by Turbulent intensity, which is set by default equal to 5%. The turbulent viscosity ratio, in other words the proportion of turbulence viscosity to dynamic flow viscosity, is also set to its default value of 10%.

In order to simulate rain, the Discrete Phase Model was enabled. The water droplets are injected from a rectangular surface, at 15m upstream the blade, in order to reduce computational memory and computational time. The horizontal velocity of the water droplets is equal to the air flow velocity and the vertical velocity is calculated by the empirical equation of Markowitz, taking into account the droplet diameter [30]. The Taylor Analogy Breakup (TAB) model is also enabled for the simulation of droplets breakup as they impact the blade [31].

Five different conditions for two-phase flows over the HAWT rotor were examined, for various LWCs and various droplet diameters, as they are presented in Figure 4.

The velocity and pressure values are updated simultaneously through the option "coupled" at Pressure-Velocity Coupling. The "Least Square Sell Based" model is selected for the discretization of the Gradient coefficients and the "standard" model is selected for the Pressure discretization. The "second order upwind" model is used for the discretization of momentum values, while the "first order upwind" is used for the discretization of Turbulent Kinetic Energy and Specific Dissipation Rate. The "Pseudo Transient" and "High Order Term Relaxation" mechanisms are used to control the convergence of variables.

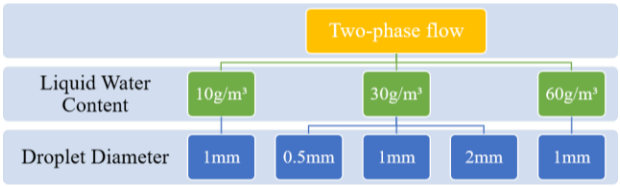

Figure 4. The examined conditions for the two-phase flow

III. Computational Results

III.1. One-phase flow of air

Prior to the study of the rainfall, the air flow around the wind turbine blade should be examined, in order to estimate the effect of rain by the comparison of the results of the two different conditions. The velocity of the air for the simulations was equal to15m/s and for the tip speed ratio a typical value of 6 was selected.

The present model cannot be validated directly, since corresponding experimental data do not exist. Due to this lack of experimental data for a wind turbine rotor of similar size, the specific aerodynamic performance was compared with the performance of a commercial rotor of a similar size, to appraise the estimated results. The power coefficients of three commercial wind turbines were compared with the power coefficient of the blade of the present study and the results are presented in Table 1. Specifically, the wind turbines studied are the General Electric three-bladed wind turbines GE 1.85 – 87 [32] and GE 2.5 – 88 [33].

Table 1. Power coefficient of commercial wind turbines and comparison with the numerical results of the three-bladed wind turbine with blade constructed by NACA 4418 airfoil

Wind Turbine Model	Swept area (m^2)	Rated wind speed (m/s)	Rated power (MW)	Power Coefficient Cp	Deviation of Power Coefficient (%)
GE 1.85 – 87	5346	13	1.85	0,257	10,95
GE 2.5 – 88	6082	14	2.50	0,244	6,36

It is apparent that the deviation of the calculated Power Coefficient is comparatively low, which means that the computational method is reliable. The factor that can affect the difference in performance from commercial models is the different geometry, as blades consisting of only one type of airfoil, as considered in present work, are rarely used in the market.

In Figure 5 the static pressure distribution on the pressure and the suction side of the blade, for air flow, is presented. The magnitude of static pressure receives its highest absolute value on the suction side of the blade, in about 30% of its length, close to the tip. Moreover, static pressure values are also high in the pressure side of the blade, close to the leading edge of the airfoil, but these values are lower than the negative values on the suction side. The pressure difference between the two sides of the blades is responsible for lift generation, which is responsible for the rotation of the blade.

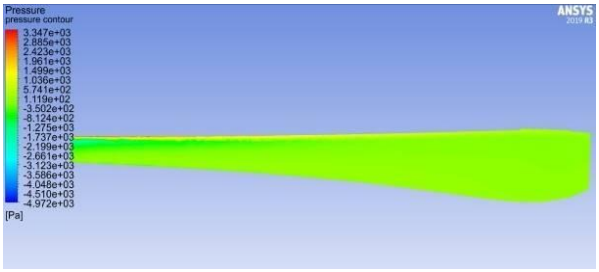

(a)

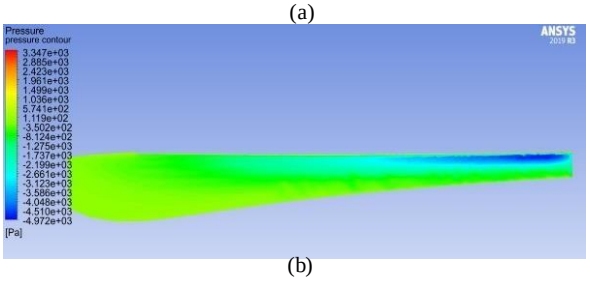

(b)

Figure 5. Static pressure distribution on (a) the pressure and (b) the suction side of the NACA 4418 blade for air flow

Figure 6 shows the relative velocity vectors at various sections along the blade, from close to the hub up to close to the tip. The velocity values are lower at the stagnation point and they are even lower for the sections close to the hub. The velocity reaches its highest values on the upper side of the airfoil, and in particular at the region between the leading edge and the middle of the airfoil, for all sections. The region with the highest values of velocity follows the region where the flow is separated, because of the gradual reduction of the air velocity due to friction. The separated flow expands at greater regions as the airfoil sections are closer to the blade tip.

In Figure 7 the static pressure distribution around the airfoil at various sections along the blade are presented. It is obvious that the static pressure difference between the suction and pressure surface of the blade increases along the blade, as we are moving from the hub towards the blade tip.

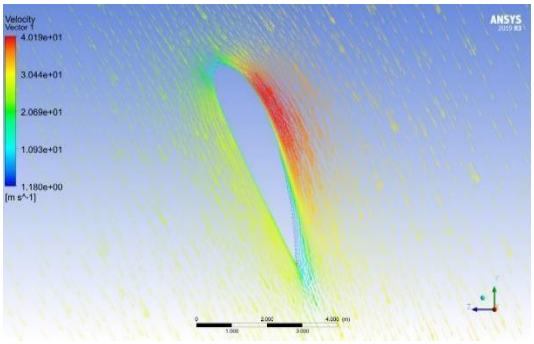

(a)

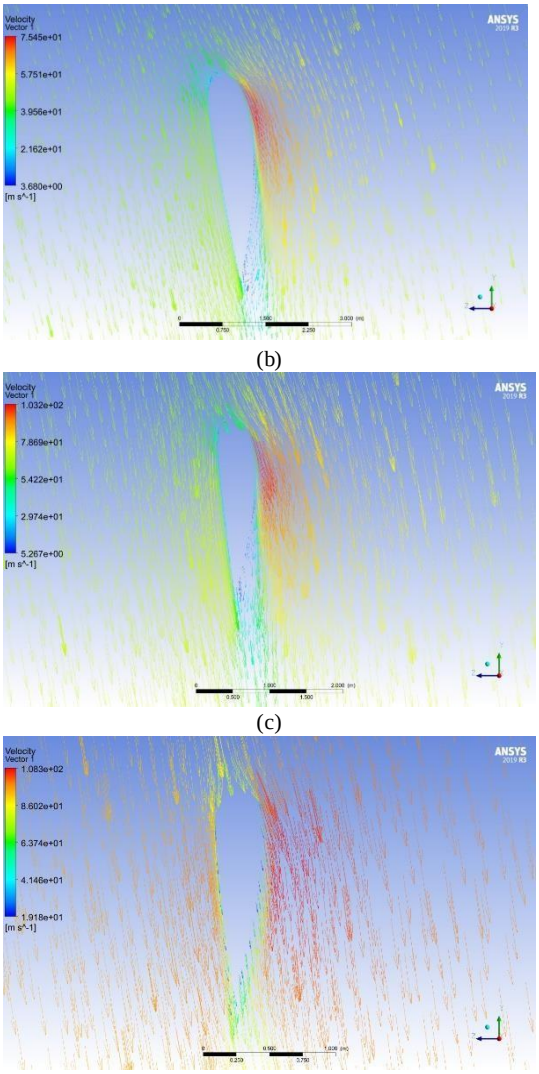

Figure 6. Relative velocity vectors around various blade sections at a distance (a) r/R=0.25, (b) r/R=0.50, (c) r/R=0.75 and (d) r/R=0.99 from the rotor hub

However, the maximum pressure difference along the blade occurs at r/R=0.75. Moreover, the static pressure distribution shows that the lowest pressure values appear in the regions where the velocity takes its highest values. Generally, it is observed that the pressure is reduced in the regions where the velocity is increased and vice versa, which is confirmed by Bernoulli's equation.

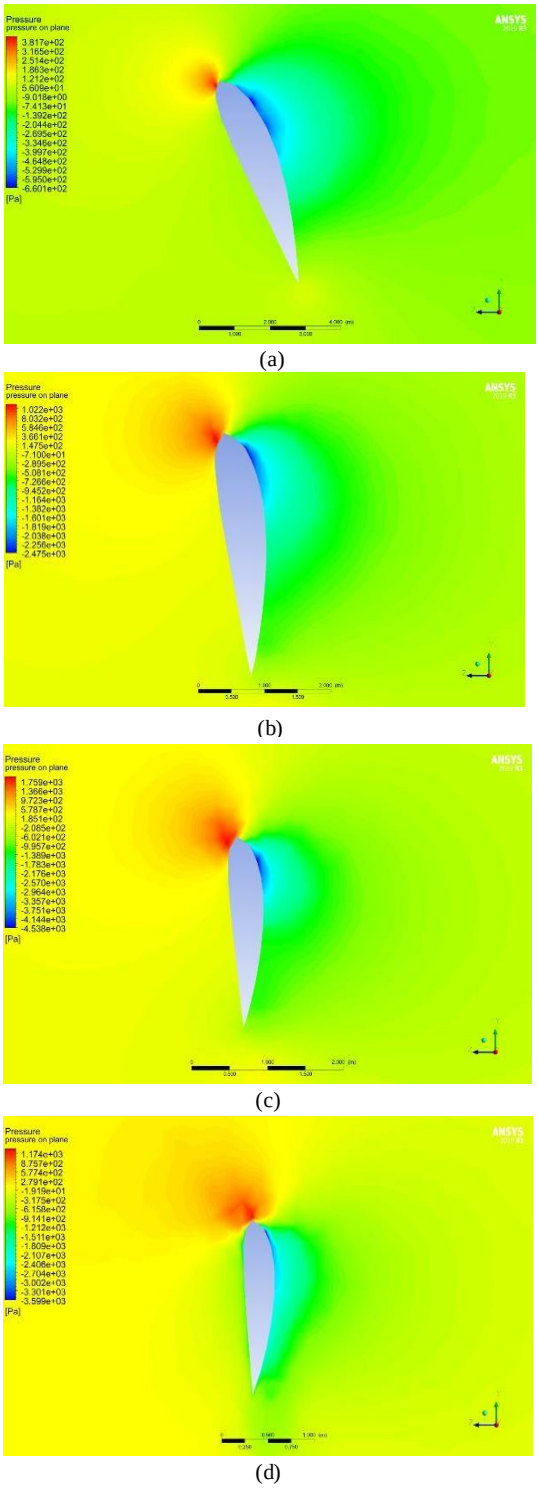

Figure 7. Static pressure distribution around various blade sections at a distance (a) r/R=0.25, (b) r/R=0.50, (c) r/R=0.75 and (d) r/R=0.99 from the rotor hub

III.2. Two-phase flow of air and water droplets

In order to show the effect of rainfall on the aerodynamic performance of the HAWT rotor, three different Liquid Water Contents (LWCs) were examined,

and in particular 10g/m^3, 30g/m^3, and 60g/m^3, which represent light, medium and heavy rainfall, respectively.

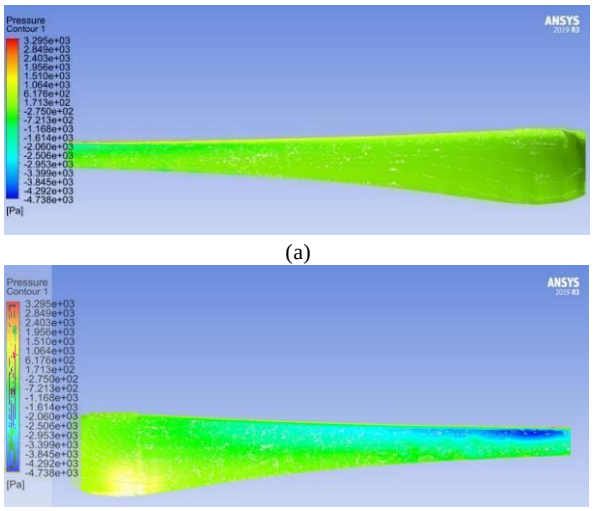

(a)

(b)

Figure 8. Static pressure distribution on (a) the pressure and (b) the suction side of the NACA 4418 blade for LWC=10g/m^3

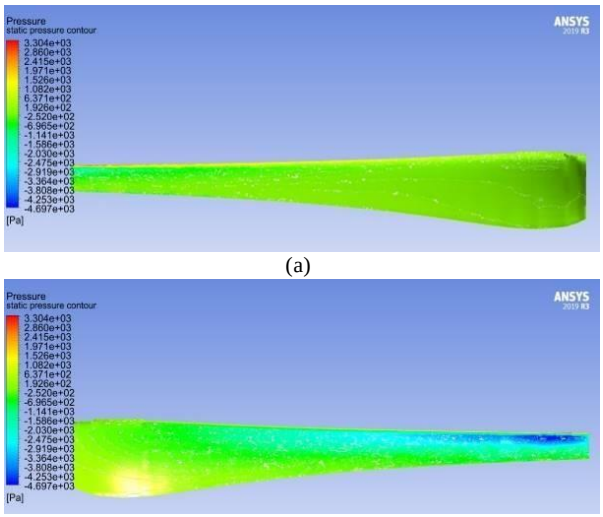

(a)

(b)

Figure 9. Static pressure distribution on (a) the pressure and (b) the suction side of the NACA 4418 blade for LWC=30g/m^3

From Figure 8 to Figure 10 the static pressure distribution on the suction and the pressure side of the blade under light, medium and heavy rainfall, is presented. The pressure distribution is the same as for the one-phase flow, i.e. the highest absolute value of the static pressure is located on the suction side of the blade. Furthermore, the minimum values of the static pressure are increased as the LWC increases. More specifically, the minimum static pressure is increased compared to the corresponding one-phase flow by 4.7%, 5.5% and 8% for LWCs of 10g/m^3, 30g/m^3, and 60g/m^3, respectively.

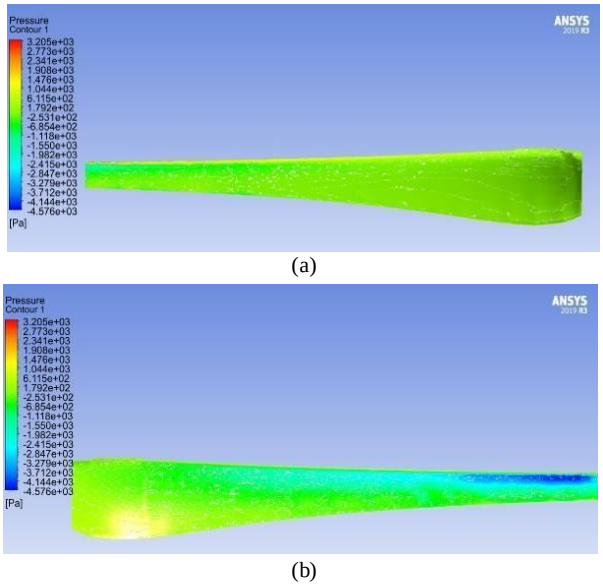

(a)

(b)

Figure 10. Static pressure distribution on (a) the pressure and (b) the suction side of the NACA 4418 blade for LWC=60g/m^3

In Figure 11 and Figure 12 the water film height on the pressure and the suction side of the blade, for the three different LWCs that were examined, is illustrated.

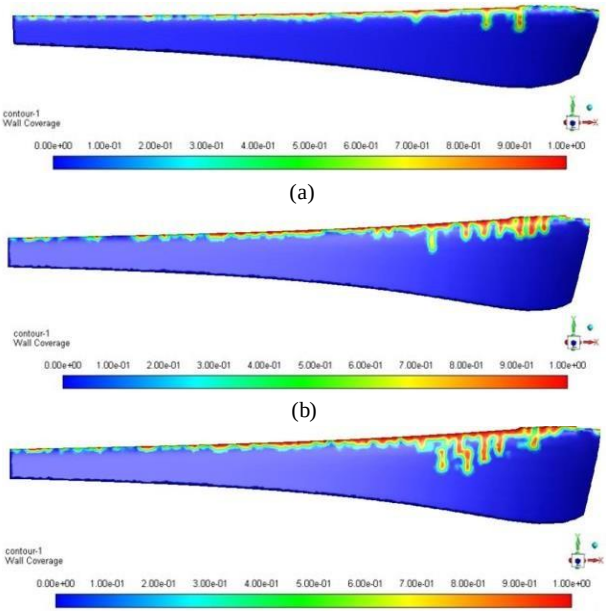

(a)

(b)

(c)

Figure 11. Water film height on the pressure side of the blade for LWC of (a) 10g/m^3, (b) 30g/m^3 and (c) 60g/m^3

It can be observed that the maximum water film thickness is located close to the hub, where the chord length of the blade is greater, whereas less quantity of water is concentrated close to the blade tip. This could be explained by the fact that centrifugal force tends to remove the water from the blade. Moreover, from these

Figures it is clear that the water film occupies more space on the blade for higher LWC values.

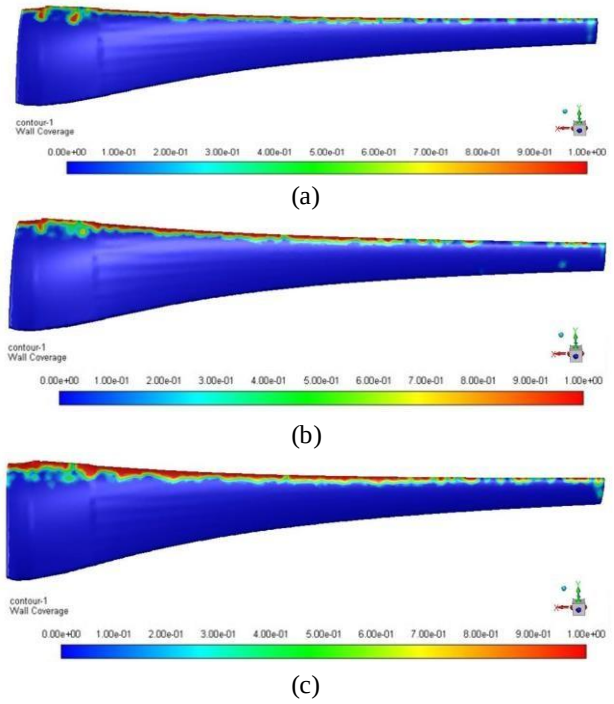

Figure 12. Water film height on the suction side of the blade for LWC of (a) 10g/m^3, (b) 30g/m^3 and (c) 60g/m^3

Table 2 shows the calculated power coefficient and of the examined HAWT and the degradation of power coefficient due to rain, for all the LWCs that were simulated, and for water droplet diameter equal to 1mm. Moreover, the mass flow rate of the water that impacts the blade is provided in Table 2. Figure 13 shows the power coefficient of the wind turbine versus the LWC and there is a clear trend of almost linearly decreasing of power coefficient as the LWC increases.

Table 2. Calculated power coefficient and its degradation due to rain conditions, and water mass flow rate on the blade

LWC (g/m^3)	Water mass flow rate on the blade (kg/s)	Power Coefficient Cp	Degradation of Power Coefficient (%)
0	0.0	0.223	---
10	4.5	0.199	10.8
30	14.0	0.190	14.8
60	20.0	0.174	22.0

Figure 13. Power coefficient of the wind turbine at different LWCs

These results are in line with the theoretical estimation that rainfall has adverse effects on the performance of a wind turbine. As the density of the rainfall increases, the water film on the blade is thicker and the cratering effects from the raindrops impact are more intense, leading in higher aerodynamic drag.

The impact of droplet diameter on the aerodynamic degradation of a HAWT was examined as well. Three different droplet diameters, of 0.5mm, 1mm and 3mm were simulated, for LWC=30g/m³ and air velocity equal to 15m/s. Figure 14 and Figure 15 present the water film height on the pressure and the suction side of the blade, for the three different droplet diameters that were examined, for constant LWC and equal to 30g/m³. From these Figures it is apparent that there is an increase in water concentration on the blade surface with an increase in droplet diameter and the highest water film appears to develop in the area close to the hub, for all three cases. This phenomenon could be explained by the fact that droplets of larger diameter are most probably unaffected by local aerodynamic forces and they follow a more direct path due to their greater mass and inertia. In contrast, droplets with smaller diameters are more vulnerable to these forces and may never reach the body.

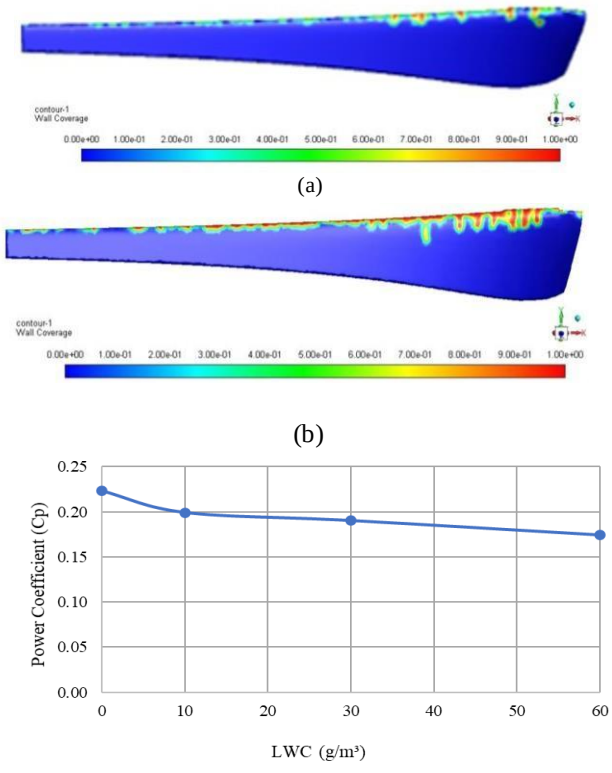

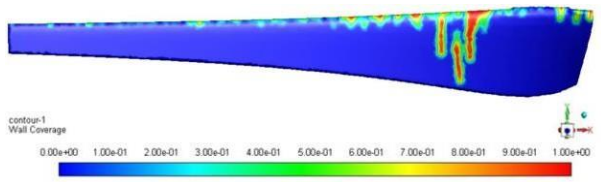

(c)

Figure 14. Water film height on the pressure side of the blade for LWC of 30g/m^3 and droplet diameter of (a) 0.5mm, (b) 1mm and (c) 2mm

Table 3 and Figure 16 show the results of power coefficient for LWC=30g/m³ and different droplet diameters. It is obvious that the performance of the wind turbine is negatively affected by the diameter of the rain droplets. However, it is observed that this reduction is smaller than the corresponding one due to the increase of LWC in the flow.

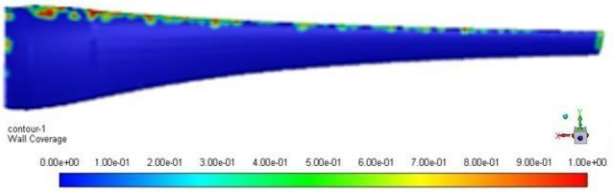

(a)

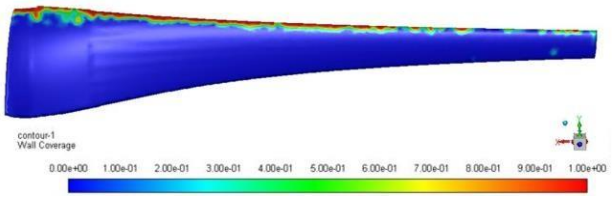

(b)

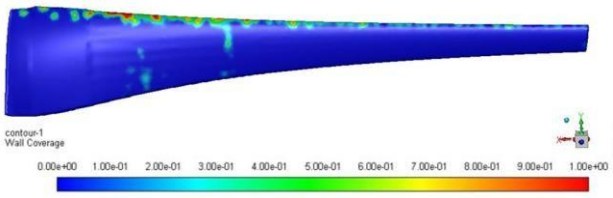

(c)

Figure 15. Water film height on the suction side of the blade for LWC of 30g/m^3 and droplet diameter of (a) 0.5mm, (b) 1mm and (c) 2mm

Table 3. Calculated power coefficient and its degradation for LWC of 30g/m³ and different droplet diameters

Droplet Diameter (mm)	Power Coefficient Cp	Degradation of Power Coefficient (%)
0	0.223	---
0.5	0.196	12.3
1.0	0.190	14.8
2.0	0.187	16.0

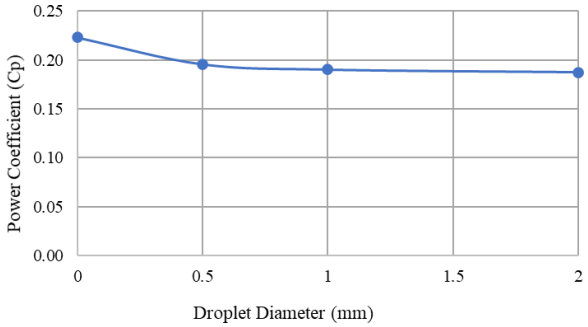

Figure 16. Power coefficient of the wind turbine for LWC=30g/m³ and different droplet diameters

IV. Conclusion

The purpose of the current study was to determine the effects of rainfall on the aerodynamic performance of a HAWT with blades constructed by NACA 4418 airfoil. Initially, the one-phase flow of air was studied and then the two-phase flow of air and water droplets, in order to compare the results and understand the impact of rain on the HAWT performance.

From the contours of static pressure it was found that the highest absolute value of static pressure appears on the suction side of the blade, close to the tip, for all the cases studied, both for air flow and rainfall conditions. Moreover, the static pressure difference between the pressure and the suction surface of the blade increases along the blade, towards the blade tip.

In rainfall conditions, the lowest negative values of static pressure were increased with the LWC of 10g/m^3, 30g/m^3, and 60g/m^3, by 4.7%, 5.5% and 8%, respectively. It can be observed that the maximum water film thickness is located close to the hub, where the chord length of the blade is greater, whereas less quantity of water is concentrated close to the blade tip, because the centrifugal force tends to remove the water from the blade. Moreover, it is clear that the water film occupies more space on the blade for higher values of LWC.

Furthermore, a significant degradation of the aerodynamic efficiency of the compared to the one-phase flow was observed, equal to 11.84%, 16.87% and 23.9% for rain densities of 10g/m^3, 30g/m^3, and 60g/m^3 respectively.

Finally, the increase in the diameter of the raindrops leads to more concentration of liquid mass on the blade and at the same time a degradation of its aerodynamic performance since. For diameters of 0.5mm, 1mm and 2mm in a two-phase flow with LWC=30g/m^3, the reduction of the power coefficient was 15.33%, 16.87% and 17.99% respectively.

References

[1] International Energy Agency, "Global Energy & CO2 Status Report 2019", IEA, Paris, 2019.

[2] European Council, "Energy Roadmap 2050", Brussels, 2011.

[3] World Wind Energy Association (WWEA), "Wind Energy International", [Online]. Available: https://library.wwindea.org/global-statistics/. [Accessed March 2021].

[4] Y. Du, S. Zhou, X. Jing and Y. Peng, "Damage detection techniques for wind turbine blades: A review", Mechanical Systems and Signal Processing, Vol. 141, 2020.

[5] L. Mishnaevsky, K. Branner, H. Petersen, J. Beauson, M. McGugan and B. Sørensen, "Materials for Wind Turbine Blades: An Overview", Materials, Vol. 10, Issue 11, 2017.

[6] A. Miller, B. Chang, R. Issa and G. Chen, "Review of computer-aided numerical simulation in wind energy", Renewable and Sustainable Energy Reviews, Vol. 25, 2013, pp. 122-134.

[7] T. Uchida and Y. Ohya, "Micro-siting technique for wind turbine generators by using large-eddy simulation", Journal of Wind Engineering and Industrial Aerodynamics, Vol. 96, Issue 10-11, 2008, pp. 2121-2138.

[8] J. Palma, F. Castro, L. Ribeiro and A. Ro, "Linear and nonlinear models in wind resource assessment and wind turbine micro-siting in complex terrain", Journal of Wind Engineering and Industrial Aerodynamics, Vol. 96, Issue 12, 2008, pp. 2308-2326.

[9] M. Song, K. Chen, Z. He and X. Zhang, "Wake flow model of wind turbine using particle simulation", Renewable Energy, Vol. 41, 2012, pp. 185-190.

[10] J. Prospathopoulos, E. Politis and P. Chaviaropoulos, "Application of a 3D RANS solver on the complex hill of Bolund and assessment of the wind flow predictions", Journal of Wind Engineering and Industrial Aerodynamics, Vol. 107–108, 2012, pp. 149-159.

[11] B. Kim, W. Kim, S. Lee, S. Bae and Y. Lee, "Developement and verification of a performance based optimal design software for wind turbine blades", Renewable Energy, Vol. 54, 2013, pp. 166-172.

[12] C. Baxevanou, P. Chaviaropoulos, S. Voutsinas and N. Vlachos, "Evaluation study of a Navier–Stokes CFD aeroelastic model of wind turbine airfoils in classical flutter", Journal of Wind Engineering and Industrial Aerodynamics, Vol. 96, Issue 8–9, 2008, pp. 1425-1443. C. Thumthae and T. Chitsomboon, "Optimal angle of attack for untwisted blade wind turbine", Renewable Energy, Vol. 34, Issue 5, 2009, pp. 1279-1284.

[13] S. Rajakumar and D. Ravindran, "Iterative approach for optimising coefficient of power, coefficient of lift and drag of wind turbine rotor", Renewable Energy, Vol. 38, Issue 1, 2012, pp. 83-93.

[14] D. Douvi and D. Margaris, "Numerical simulation of NACA 0012 airfoil in air phase flow and in high concentration air–sand particles two-phase flow", in 8th International Conference from "Scientific Computing to Computational Engineering", Athens (Greece), July 4-7 2018.

[15] D. Douvi, D. Margaris and A. Davaris, "Aerodynamic Performance of a NREL S809 Airfoil in an Air–Sand Particles Two Phase Flow", in 7th International Conference "Scientific Computing to Computational Engineering", Athens (Greece), July 6-9 2016.

[16] I. Zidane, K. Saqr, G. Swadener, X. Ma and M. Shehadeh, "Computational Fluid Dynamics Study of Dusty Air Flow Over NACA 63415 Airfoil for Wind Turbine Applications", Jurnal Teknologi, Vol. 79, Issue 7-3, 2017, pp. 1-6.

[17] R. Rhode, "Some Effects on Rainfall on Flight of Airplanes and on Instrument Indications", NACA TN 803, 1941.

[18] A. Bilanin, "Scaling Laws for Testing of High Lift Airfoils Under Heavy Rainfall", in AIAA 23rd Aerospace Science Meeting, Reno, NV, U.S.A, January 1985.

[19] E. Douvi and D. Margaris, "Aerodynamic Performance Investigation under the Influence of Heavy Rain of a NACA 0012 Airfoil for Wind Turbine Applications", International Review of Mechanical Engineering (I.RE.M.E.), Vol. 6, Issue 6, 2012, pp. 1228-1235.

[20] E. Douvi, D. Margaris, S. Lazaropoulos and S. Svanas, "Experimental and Computational Study of the Effects of Different Liquid Water Content on the Aerodynamic Performance of a NACA 0012 Airfoil at Low Reynolds Number", in 5th International Conference "on Experiments/ Process/ System Modeling/ Simulation/ Optimization", Athens (Greece), 2013.

[21] E. Douvi, D. Margaris, S. Lazaropoulos and S. Svanas, "Low Reynolds Number Investigation of the Flow over a NACA 0012 airfoil at Different Rainfall Rates", International Review of Mechanical Engineering (I.RE.M.E.), Vol. 7, Issue 4, 2013, pp. 625-632.

[22] R. Corrigan and R. DeMiglio, "Effect of Precipitation on Wind Turbine Performance", NASA-TM-86986, 1985.

[23] H. Glauert, "The Theory of the Autogyro", The Journal of the Royal Aeronautical Society, vol. 31, Issue 198, 1927, pp. 483-508.

[24] ANSYS®, Academic Research, Release 19.2.

[25] E. Douvi and D. Margaris, "Hydrodynamic Analysis of a Horizontal Axis Tidal Turbine, Based on the Blade Element Momentum Theory", in Proceedings of the 7th International Conference on "Experiments/ Process/ System Modeling/ Simulation/ Optimization", Athens (Greece), July 5-8 2017.

[26] D. Marten, J. Wendler, G. Pechlivanoglou, C. Nayeri and C. Paschereit, "QBlade: An Open Source Tool for Design and Simulation of Horizontal and Vertical Axis Wind Turbines", International Journal of Emerging Technology and Advanced Engineering, Vol. 3, 2013, pp. 264–269.

[27] J. Y. Luo, R. I. Issa and A. D. Gosman, "Prediction of impeller induced flows in mixing vessels using multiple frames of reference", in 8th European conference on mixing, Cambridge, 1994.

[28] F. Menter, "Two-Equation Eddy-Viscosity Turbulence Models for Engineering Applications", AIAA Journal, Vol. 32, 1994, pp. 1598-1605.

[29] A. Markowitz, "Raindrop Size Distribution Expression", Journal of Applied Meteorology, Vol. 15, 1976, pp. 1029-1031.

[30] G. Taylor, "The Shape and Acceleration of a Drop in a High Speed Air Stream", In the Scientific Papers of G. I. Taylor, ed., G. K. Batchelo, 1963.

[31] GE Renewable Energy, "Capacity Factor Leadership in Class S Winds, GE's 1.85 - 87", General Electric, 2013.

[32] https://www.ge.com/renewableenergy/sites/default/files/related_documents/wind-onshore-turbine-1.85-87-gea30627d-r1.pdf

[33] GE Power & Water Renewable Energy, "2.5MW Wind Turbine Series", General Electric, 2013.